


Automatic Detection of Systemic Diseases to Recognize Mpox Virus using GPLNet Based on Skin Lesions


Panji Bintoro

(Software Engineering, Faculty of Technology and Informatics, Aisyah University, Indonesia
 <https://orcid.org/0000-0002-2955-1872>, panjibintoro09@aisyahuniversity.ac.id)


Zulkifli Zulkifli

(Informatics Engineering, Faculty of Technology and Informatics, Aisyah University, Indonesia,
 <https://orcid.org/0000-0002-8702-0885>, zulkifli@aisyahuniversity.ac.id)


Yaya Heryadi

(Department of Computer Science, BINUS Graduate Program-Doctor of Computer Science, Bina Nusantara University, Jakarta, Indonesia,
 <https://orcid.org/0000-0001-7966-2573>, yayaheryadi@binus.edu)


Fitriana Fitriana

(Midwifery, Faculty of Health, Aisyah University, Indonesia,
 <https://orcid.org/0000-0003-3230-2591>, fitriana@aisyahuniversity.ac.id)

Nopi Anggista Putri

(Midwifery, Faculty of Health, Aisyah University, Indonesia,
 <https://orcid.org/0000-0002-2323-637X>, nopianggista@aisyahuniversity.ac.id)

Dwi Yana Ayu Andini

(Software Engineering, Faculty of Technology and Informatics, Aisyah University, Indonesia
 <https://orcid.org/0000-0001-6748-6330>, dwiyana@aisyahuniversity.ac.id)

Abstract: Mpox is a disease like smallpox caused by the Mpox virus (MPXV), which belongs to the Orthopoxvirus (OPXV) group in the Poxviridae family. The virus is transmitted through direct contact with infected individuals, animals, or contaminated materials. Transmission can occur through direct body contact, animal bites, respiratory droplets, or mucous membranes in the eyes, nose, or mouth. However, since the recent outbreak in May 2022, the disease has spread to various countries, posing a threat to develop into a global pandemic. Several image processing and deep learning models, including Convolutional Neural Network (CNN), have been employed for Mpox disease prediction. The default CNN algorithm performs poorly on image orientations such as tilting, rotation, zooming, or other abnormal images. Therefore, we propose a new framework adopted from deep learning by combining Generative Adversarial Network (GAN), PyramidalNet, and Long Short-Term Memory (LSTM). This new method is referred to as GPLNet. The research results indicate that the GPLNet algorithm model can surpass the accuracy achieved by CNN and CNN-LSTM, reaching 99%. The performance of the GPLNet algorithm model is also evaluated using various measurement metrics, yielding an accuracy of 98%, precision of 99%, recall of 98%, sensitivity of 98%, specificity of 98%, f1-score of 98%, and ROC of 99%.

Keywords: Sytemic Disease, Mpox, Skin Lesions, CNN, LSTM, GPLNet

Categories: I.5.1, I.5.2, I.5.4, I.5.5

DOI: 10.3897/jucs.119234

1 Introduction

Since the outbreak of the corona virus disease (COVID-19) in 2019 [Chen et al., 20, Stojanov, 23], there remains a threat of the emergence of an epidemic [Stojanov, 21] caused by the Mpox virus prompted health experts to collectively question whether this could pose new risks [Akkilic et al., 24]. ¹Monkeypox or Mpox, a disease similar to smallpox caused by the Mpox virus, primarily originates from the Central and West African regions [Chadaga et al., 23]. The Monkeypox virus (MPXV) is part of the Orthopoxvirus (OPXV) group within the Poxviridae family [Arden and Chilcot, 20]. Poxviruses are large-sized viruses with an envelope. Their genome consists of double-stranded linear DNA (~200 kilobase pairs), densely packed with around ~200 genes [Xiang and White, 22]. The complete genome of MPVX, the first isolated from the current MPVX outbreak (designated as MPVX_U.S._2022_MA001), was released in the GenBank database with the accession ID ON563414 as of May 30, 2022 [Gigante et al., 22]. Oxford nanopore technology revealed that the size of the MPVX genome is 197,205 bp as linear dsDNA. The average size of MPVX ranges between 200 and 250 nm. MPVX replicates in the cytoplasm of infected host cells and possesses a nuclear region with lateral bodies, double-stranded DNA (dsDNA), and a lipoprotein envelope [Karagoz et al., 23].

Micropinocytosis, virus endocytosis, and cell membrane fusion facilitate virus entry through the nasopharyngeal, oropharyngeal, subcutaneous, intradermal, and intramuscular routes. Inflammatory immune-mediated phagocytosis is triggered by MPXV replication upon inoculation, leading to MPXV spread to the blood, lymph nodes, tonsils, bone marrow, spleen, and other organs. MPXV genome and proteins are released into host cells under the control of mature virions (MV) and enveloped virions (EV). Following MPXV mRNA transcription and translation, intracellular mature virions (IMV) with the virus-coding DNA are produced. IMVs wrapped in Golgi apparatus-derived membranes create intracellular enveloped virions (IEVs), which fuse with the host cell's inner membrane to form cell-associated virions (CEVs) before being released into the extracellular area to form extracellular enveloped virions (EEV) [Paharia, 22]. The virus is transmitted when an individual has direct contact with infected people, animals, or contaminated materials [Ahsan, et al., 23]. Transmission can occur through direct bodily contact, animal bites, respiratory droplets, or mucous membranes in the eyes, nose, or mouth [Nguyen et al., 21]. However, since the recent outbreak in May 2022, the disease has spread to various countries, posing a threat to develop into a global pandemic [Hemati et al., 22].

The OPXV genus has more than 10 member species, including the variola virus (smallpox) (VARV) [Altun et al., 23], vaccinia virus (VACV) [Dhungel et al., 20], cowpox virus (CPXV) [Velu et al., 23], camelpox virus (CMLV) [Zhugunissov et al., 23], and several new species isolated from infected humans or primates since 2010 [W.

¹ The use of the term "Monkeypox" in the related works section is because the term is used in the references.

T. Yang et al., 22]. In 2018, there was an outbreak suspected to be monkeypox in an 11-year-old child, and the disease was considered a threat [Jaradat et al., 23]. As of January 1, 2019, 132 confirmed cases of the disease and 7 deaths were reported. On June 23, 2022, the World Health Organization (WHO) reported more than 3000 monkeypox virus infections in over 50 countries across five regions [Dimitrakoff et al., 22].

Several studies related to the detection of monkeypox disease have been conducted, one of which was carried out by [Bala et al., 23] to discuss a powerful Deep Convolutional Neural Network for the detection and classification of monkeypox disease. Additionally, [Altun et al., 23] also investigated the detection of monkeypox using a Convolutional Neural Network that employs a Transfer Learning approach.

Systemic disease detection aims to identify monkeypox disease by integrating variables into the dataset such as swollen lymph nodes [Pittman et al., 22], muscle pain [Studemeister et al., 23], and fever [Baudouin et al., 2023, Chastain et al., 2023]. Systemic disease utilized for identifying monkeypox is based on variables such as anal pain [Pfäfflin et al., 23], sore throat [Ardila et al., 23], penile swelling [Valero, 23], mouth lesions [Joseph & Anil, 23], solitary lesions [Mitjà et al., 23], swollen tonsils [Karagoz et al., 23], HIV infection [Ethawi et al., 23], and sexually transmitted infections [Allan-Blitz & Klausner, 23]. From these variables, a dataset is formed to detect systemic disease for identifying monkeypox using the (GAN - Pyramidal - LSTM Network) GPLNet model based on skin lesions. Applications utilizing deep learning can be assessed through data analysis parameters such as precision, recall, f-measure, and ROC.

This research proposes the GPLNet model for systemic disease detection to identify Mpox. The creation of the GPLNet model, which not only focuses on the end results but also considers the original and fake input images, training speed, and network stability, is a significant contribution made in this study. The remainder of this research is divided into several sections such as Related Works presented in Section 2, research materials and methodology, along with the workflow shown in Section 3. Experiments and their results are presented in Section 4. In Section 5, conclusions are drawn and future work concludes in Section 6.

2 Related Works

Several preliminary studies have been conducted on Mpox cases. In a study by [Dahiya et al., 23], CNN with transfer learning was employed for the detection of monkeypox disease. Researchers preprocessed skin image data from mobile devices before it could be trained or tested. The data was divided into 70% for training and 30% for validation. The data was categorized into two groups, namely positive and negative for monkeypox. Custom models such as MobileNetV3-s, EfficientNetV2, ResNET50, Vgg19, DenseNet121, and Xception models were implemented in this research. In the research, the evaluation and comparison involved metrics such as Area Under Curve (AUC), accuracy, recall, loss, and F1-score. The MobileNetV3-s hybrid model, after optimization, demonstrated superior performance, attaining the highest scores across various parameters, including an average F1-score of 0.98, AUC of 0.99, accuracy of 0.96, and precision of 0.97. The diagnosis of melanoma disease investigated by [Nivedha & Shankar, 23] utilizes a Faster Region Convolutional Neural Network

optimized with the Artificial Gorilla Troop Algorithm. This research aims to reduce the complexity of the analytical process, selecting valuable features using the AGTO method, and further classification implemented using Faster R-CNN. The study demonstrates that the proposed system outperforms existing models with an accuracy of 98.55%. Lesion-based skin disease diagnosis is also conducted by [Hussain et al., 23], where the study proposes a controlled positive correlation approach for the fusion of trained neural network features and an enhanced optimization development named Antlion for feature selection. The research utilizes the ISIC2018 skin dataset consisting of 10,014 images distributed across 7 classes and ISIC2019 consisting of 23,757 images distributed across 8 classes. In its experimental process, it achieves accuracies of 96.1% and 99.9%, respectively.

Detection and classification using a deep learning-based feature selection and fusion approach are conducted by [Maqsood & Damaševičius, 23]. In their research, a contrast enhancement-based fusion approach is utilized for image preprocessing. The DCNN model proposed in the study achieves an accuracy of 98.59%, sensitivity of 92.78%, specificity of 95.47%, and an AUC of 0.987. Detection of monkeypox virus using a deep learning-based approach is also conducted by [Sitaula & Shahi, 22]. The research aims to compare 13 different deep learning models for monkeypox virus detection. In conducting experiments on the available dataset, it yields average Precision, Recall, F1-score, and accuracy of 85.44%, 85.47%, 85.40%, and 87.13%, respectively, with the assistance of the proposed approach.

Multiclass skin lesion recognition using the MSRNet approach is conducted by [Bibi et al., 23]. The research proposes a deep learning architecture for multiclass skin cancer classification and melanoma detection. The proposed architecture consists of 4 stages: image processing, feature extraction and fusion, feature selection, and classification. Two datasets, ISIC2018 and ISIC2019, were chosen for the experimental process. The maximum accuracies obtained on these datasets are 85.4% and 98.80%, respectively.

The research conducted by [Azar et al., 23] developed seven specifically designed Deep Convolutional Networks (DNN) to detect monkeypox, considering both two-class and four-class scenarios. The results of the study indicate that the proposed DenseNet201-based architecture performs the best, with an accuracy of 97.63%, F1-score of 90.51%, and AUC of 94.27% in the two-class scenario, while achieving an accuracy of 95.18%, F1-score of 89.61%, and AUC of 92.06% in the four-class scenario. Utilizing deep learning approaches such as GoogLeNet, Places365-GoogLeNet, SqueezeNet, AlexNet, and ResNet-18, [Nayak et al., 23] focused on image-based lesion detection for monkeypox virus using publicly available datasets. The aim of the research was to explore how the models could be employed in real-time or for accurate diagnosis. ResNet-18 achieved the highest accuracy of 99.49%, while the modified model attained validation accuracy above 95%. The results demonstrate that deep learning models, such as the proposed one based on ResNet-18, can be applied, and play a crucial role in combating the monkeypox virus.

The research conducted by [Ijaz et al., 23] focuses on the detection of monkeypox in humans using deep learning. This study proposes the Long Short-Term Memory (LSTM) algorithm to analyze periodic symptom records or patient data, while the Convolutional Neural Network (CNN) algorithm is used to process medical images of skin lesions. The researchers divided the data for training into 70%, validation data into 15%, and testing data into 15%. The data is categorized into two classes, namely positive and negative for monkeypox. The research results indicate that the proposed

CNN and LSTM models achieved an accuracy of 99%. The utilization of the CNN model for monkeypox classification based on skin lesions was also performed by [Eliwa et al., 23]. This research optimized the CNN model using the Grey Wolf Optimizer (GWO) algorithm, resulting in a significant improvement in accuracy, precision, recall, F1-score, and AUC compared to the non-optimized model. The optimized CNN model achieved an accuracy of 95.3%, demonstrating that the GWO optimizer enhanced the model's ability to differentiate between positive and negative classes.

3 The Purpose Method

3.1 Research Workflow

Figure 1 illustrates the proposed research workflow in this study, where systemic disease data based on skin lesions is utilized as input to identify Mpox.

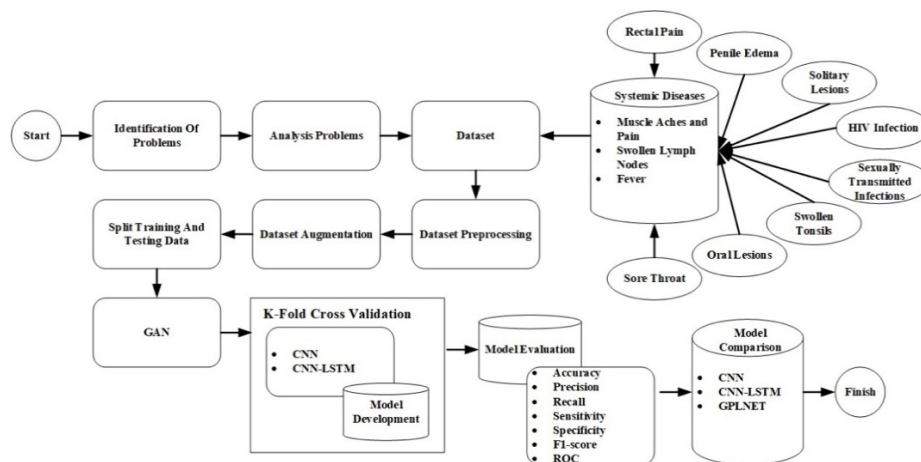


Figure 1: Research flow design

The stages of the research workflow are described as follows:

3.2 Identification of Problems

In this stage, the identification of problems includes:

- The need for an automatic detection model to recognize Mpox virus based on skin lesion.
- Measuring the accuracy level of the proposed model using both augmented and non-augmented datasets.

3.3 Analysis Problem

In this stage, the design of an automatic detection model to recognize Mpox virus based on skin lesions is conducted. The model we propose is called GPLNet (GAN - Pyramidal - LSTM Network).

3.4 Data Collection

Many experts in the field of medical health believe that artificial intelligence systems can effectively and efficiently diagnose diseases by processing image data [Ahsan et al., 20, Ahsan et al., 23]. During the initial stages of our experiment, we found only a limited collection of publicly available Mpox data, which somewhat hindered the effective and efficient implementation of the system. Considering the limitations in this research, we gathered images of patients with Mpox symptoms, and this dataset will be periodically updated with contributions from hospitals, clinics, or data obtained from internet data repositories [Paul et al., 22]. Figure 2 illustrates the results of the data collection, and Table 1 presents the characteristics of the dataset collected in this study.

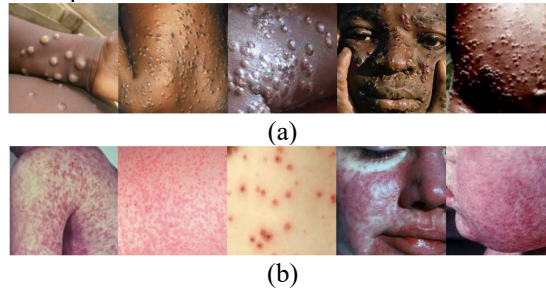


Figure 2: A collection of sample images from the data set (a) infected with monkey pox (b) not infected with monkey pox

Dataset	Total Sample
Infected Mpox	102
No Infected Mpox	126
Infected Mpox Augmented	980
No Infected Mpox Augmented	1162
Total Samples	2370

Table 1: Characteristics of the dataset that has been collected in this research

Table 1 presents the characteristics of the data collected in this study. Machine learning algorithms perform well with a small number of images, whereas deep learning algorithms such as CNN, GAN, Recurrent Neural Network (RNN) require a large amount of data to function effectively [Jiao et al., 20, Jiao & Jiang, 22, Othmani et al., 23]. Although the dataset only contains 2370 samples, using a machine learning approach, this data can be applied to build disease classification models, as demonstrated in previous research during the COVID-19 pandemic. For example, in a study that used only 100 samples to build a Deep Learning model for automatic COVID-19 classification [Mahdy et al., 22]. However, we anticipate that the data volume will increase over time as we gather more information from various open

sources, such as data that can be used without privacy concerns, information from journals, and online sources [Paul et al., 22].

3.5 Data Preprocessing and Augmentation

The primary goal of image classification using CNN is to reduce the computational complexity of the model, which may increase when the input is an image [Hussein et al., 22]. This research resized the images from 1024x1024 to 224x224 pixels to decrease the computational load and facilitate faster processing. All techniques were implemented on these reduced-size images.

In the process of deep learning algorithm classification, the imbalance ratio in the class distribution of the dataset significantly impacts the model's performance. "Data Augmentation" is a method employed in data analysis to increase the volume of data by introducing slight replicas of the existing data [Gulakala et al., 23]. In the research [Waheed et al., 20, Yang et al., 21], the authors conducted a systematic study on how data imbalance affects the CNN model's performance in classification. Their findings demonstrated the adverse impact of an imbalanced class distribution on classification performance. In our dataset, there are fewer images of mpox-infected lesions compared to images of non-infected lesions. To address this situation, we applied data augmentation to the dataset. In this study, the following parameters were used for the data augmentation process, as shown in Table 2.

Generator	Facility
Rescale	1./255
Shear range	1%
Zoom range	1%
Rotation range	15°
Fill mode	Nearest
Horizontal flip	True

Table 2: Augmentation composition technique in this research

3.6 Generative Adversarial Network (GAN)

Generative Adversarial Networks (GAN) is a deep learning algorithm that generates synthetic data from latent space, as illustrated in Figure 3. These networks draw inspiration from Ian Goodfellow and his colleagues based on contrastive noise estimation and employ the loss function used in the current GAN. Firstly, there is a generator tasked with creating new data resembling the given training data. Secondly, there is a discriminator responsible for distinguishing between real and generator-produced data [Aggarwal et al., 21]. GAN, or Generative Adversarial Network, is a model that learns to create data resembling real data by employing two adversarial networks—namely, the generator G and the discriminator D . The generator G maps a latent variable z to the data space, aiming to generate data that aligns with the distribution of real data, while the discriminator D distinguishes whether the input originates from real or generated data. D is trained to maximize the probability of assigning a value of 1 to real data and 0 to generated data from G , whereas G is trained to generate data resulting in a classification outcome of 1 [My et al., 21]. In other words, D and G engage in a two-player minimax game described by the following equation:

$$\min_G \max_D V(D, G) = \min_G \max_D \mathbb{E}_{p_x} [\log(D(x))] + \mathbb{E}_{p_{G(z)}} [\log(1 - D(G(z)))] \quad (1)$$

In equation 1, p_x represents the genuine data distribution, and $p_{G(z)}$ denotes the generated distribution, also recognized as the model distribution. The optimization of D in equation 1 creates a dilemma within D's training, presenting computational challenges and fostering overfitting on a restricted dataset. Consequently, G and D undergo alternating training, with G held constant during D's training and vice versa. Despite GAN having theoretical support and advantages, practical implementation faces the obstacle of meeting the assumption of sufficient capacity, failing to guarantee the discriminator's optimality at each optimization step. This can lead to issues like local optima entrapment and mode collapse. Numerous researchers have delved into the root causes of these problems, proposing various enhanced methods from different perspectives [Gui et al., 23]. Since the inception of GAN, diverse generator and discriminator architectures have been developed. In this study, an evolving GAN, inspired by [Li et al., 21], is presented, where both the generator and discriminator sizes increase throughout the training process.

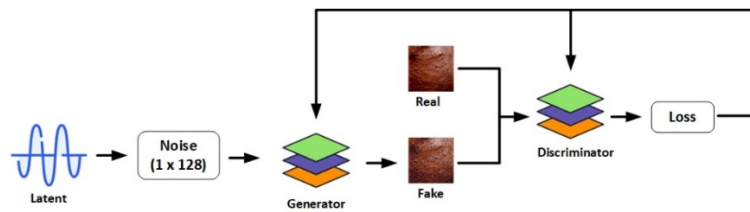


Figure 3: Generative adversarial networks

In this research, the architecture is modified to work with RGB-scale images. The fundamental concept involves employing a progressively growing number of discriminators to create high-resolution images from low-resolution counterparts. Initially, the training involves a 4×4 discriminator and generator, producing images at a 4×4 resolution. After a specified number of iterations, both the discriminator and generator layers concurrently expand to generate 8×8 images, continuing this pattern until the ultimate high-resolution image is generated. Figure 4 illustrates the GAN framework, where each block consists of two convolution layers, with each convolution followed by an LReLU activation layer.

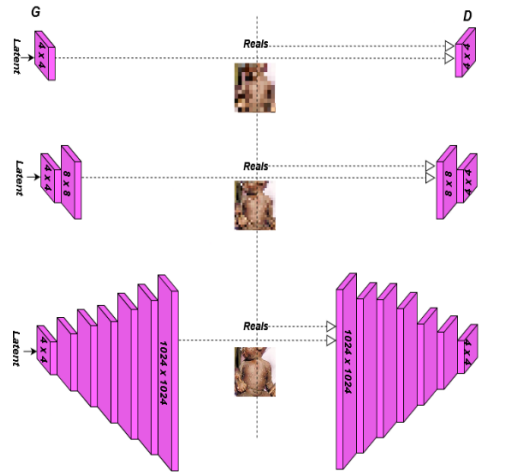


Figure 4: The framework of GAN

The upsampling and downsampling processes, along with various convolutions occurring within the generator and discriminator, are illustrated in Figure 5. To avoid sudden residual spikes into a well-trained network, a smooth transition to longer layers is incorporated. The process of increasing the resolution in both the generator and discriminator involves the gradual incorporation of new layers. When introducing a new layer, the contribution of low-resolution images (scaled up with progressively decreasing nearest-neighbor filters) and the proportion of newly generated high-resolution images steadily rise. This process is analogous to utilizing pre-trained low-level parameters for initial training, gradually incorporating, and training new layer parameters. The complete training of low-level parameters contributes to improved training stability. Moreover, as high-resolution images are incrementally produced from low-resolution counterparts, the low-resolution images acquire knowledge of large-scale structures, and high-level features act as supplementary enhancements for details and textures.

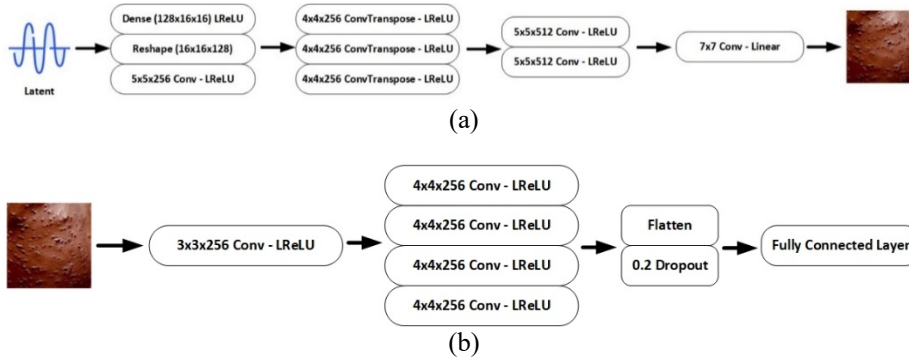


Figure 5: GAN (a) generator, and (b) discriminator blocks

This results in superior image quality and more effective training. The training progression for adding new layers from 8 x 8 to 16 x 16 is illustrated in Figure 6.

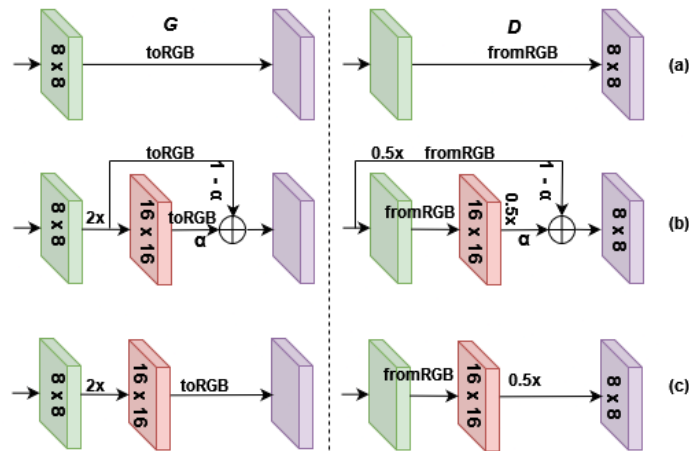


Figure 6: Training process to add new layers

The process of incorporating new layers during training involves generating high-resolution output from the newly introduced layer as a weighted residual, with the weight denoted by α . This weight scales linearly between 0 and 1 as the training advances. Subsequently, the extended low-resolution layer is scaled up using the nearest-neighbor method and combined with the residual block using a weight of $1 - \alpha$. As the training proceeds, the α value gradually increases until reaching $\alpha = 1$, obviating the need for the inclusion of longer layers. A similar procedure is applied to the discriminator, where, in this instance, the image size is halved through nearest-neighbor scaling and added to the output of the higher layer with a weight of α .

3.7 Convolutional Neural Network (CNN)

The Convolutional Neural Network (CNN) represents a progression from the Multilayer Perceptron (MLP), a neural network specifically crafted for the analysis of two-dimensional data [Eeuwijk, 22]. Like other neural networks, CNN has neurons with weights, biases, and activation functions. CNN can automatically learn hierarchical representations of input data, which are more powerful and expressive compared to manually engineered features [Eliwa et al., 23]. CNN is built from a series of sequentially added layers [Chhabra et al., 23]. Convolutional layers, pooling layers, batch normalization layers, fully connected layers, and loss layers are some of the layers that constitute these layers. These layers are part of CNN responsible for feature extraction and selection [Meena et al., 23]. There are many architectures within the CNN algorithm, such as InceptionResNetV2, InceptionV3, ResNet152V2, VGG16, VGG19, Xception, and DenseNet201 [Chai et al., 21, Jain et al., 20].

In CNN structures, as previously highlighted, the depth of feature maps escalates in successive layers owing to the stacking of numerous deep convolutional layers. Nevertheless, spatial dimensions undergo reduction since each convolutional layer or

block is succeeded by a sub-sampling layer. Therefore, deep CNNs experience a drastic increase in feature depth and, at the same time, a loss of spatial information due to the reduction in spatial dimensions. ResNet has demonstrated outstanding results for image classification problems. However, in ResNet, the removal of residual blocks, where spatial dimensions and feature maps (channels) vary (increasing feature map depth while decreasing spatial dimensions), generally degrades performance. In this case, stochastic ResNet improves performance by reducing information loss associated with the omission of residual units. We propose a method to enhance the feature map dimensions using the following equation:

$$d_l = \begin{cases} 16 & \text{if } l = 1, \\ \left\lfloor d_{l-1} + \frac{\lambda}{n} \right\rfloor & \text{if } 2 \leq l \leq n + 1, \end{cases} \quad (2)$$

Where, d_l denotes the dimension of the l^{th} residual block, and n represents the number of residual blocks, while λ is the step size, and $\frac{\lambda}{n}$ governs the increment in depth. Residual connections are inserted between layers using identity mapping without padding. The advantage of padding-free identity mapping is that it requires fewer parameters compared to projection-based shortcut connections, thus enabling better generalization. Pyramidal Net employs two different approaches to network widening, including summation and multiplication-based widening. The key difference between these types of widening is that the additive pyramid structure increases linearly, while the multiplicative pyramid structure increases geometrically.

Equation (2) relies on the summation-based widening factor λ to augment dimensions. Nonetheless, it is worth noting that multiplication-based widening, involving the multiplication of a factor to geometrically increase channel dimensions, offers an alternative approach to constructing pyramid-like structures. Consequently, Equation (2) can be reformulated as follows:

$$d_l = \begin{cases} 16 & \text{if } l = 1, \\ \left\lfloor d_{l-1} \cdot \lambda \frac{1}{n} \right\rfloor & \text{if } 2 \leq l \leq n + 1. \end{cases} \quad (3)$$

The proposed algorithm enhances feature map dimensions in all layers to distribute the concentrated load across the unit locations. It was found that using the new proposed network architecture, removing units with downsampling does not significantly decrease performance. The architecture of the multiplicative PyramidalNet is illustrated in Figure 7, where the feature map dimensions of the multiplicative PyramidalNet gradually increase geometrically, and the main contribution is that the network (PyramidalNet) focuses on increasing the feature map dimensions gradually, rather than sharply increasing them at each residual unit with downsampling. This means that the dimensions gradually increase on the input side layers and sharply increase on the output side layers.

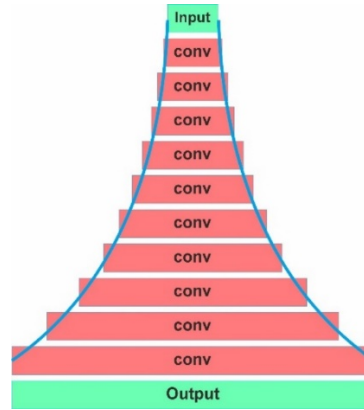


Figure 7: Multiplicative PyramidNet architecture

With the expansion of feature map dimensions in every unit of PyramidNet, we exclusively examined two alternatives: the use of an identity mapping shortcut without padding and the implementation of a projection shortcut achieved through a 3x3 convolution. The 3x3 shortcut yields results that are not suitable for very deep network architectures when there are too many residual units. Therefore, we opted for the identity mapping shortcut without padding for all residual units. In this study, identity mapping alone cannot be used as a shortcut path because the feature map dimensions differ among individual residual units. Thus, only the shortcut without padding or the projection shortcut can be used for all residual units. As explained in a prior discussion, the application of a projection shortcut could impede information propagation and lead to optimization challenges, particularly in the context of highly deep networks. Conversely, our observations revealed that the zero-padding shortcut, devoid of extra parameters, does not contribute to overfitting problems. Surprisingly, this shortcut exhibits notable generalization capabilities when compared to other shortcut methods.

We evaluated the impact of incorporating the identity mapping shortcut with zero-padding on the k -th residual unit within the n -th group using x_k^l vectors reshaped from the l -th feature map:

$$x_k^l = \begin{cases} F_{(k,l)}(x_{k-1}^l) + x_{k-1}^l, & \text{if } 1 \leq l \leq D_{k-1} \\ F_{(k,l)}(x_{k-1}^l), & \text{if } D_{k-1} < l \leq D_k \end{cases} \quad (4)$$

In equation (4), $F_{(k,l)}(\cdot)$ denotes the l -th residual function of the k -th residual unit, while D_k represents the predefined channel dimension of the k -th residual unit. The elements with zero-padding in the identity mapping shortcut for the augmented dimension, denoted as x_k^l encompass the output from both the residual network and the plain network. Therefore, we can infer that each zero-padding identity mapping shortcut can achieve this by providing a mixture of the residual network and the plain network, as shown in Figure 8. In addition to the proposed PyramidNet architecture, increasing the channel dimension at each residual unit, and the blending effect of the residual network and the plain network significantly enhances.

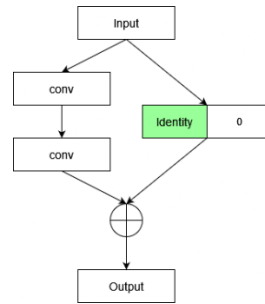


Figure 8: Residual unit structure with identity mapping shortcuts without padding

Incorporating ReLU in the construction of the residual unit block is essential for introducing nonlinearity. However, through empirical observation, we determined that its effectiveness can be influenced by the specific placement and quantity of ReLU. Notably, employing ReLU after the addition of the residual unit has a detrimental impact on performance.

$$\mathbf{x}_k^l = \text{ReLU}(\mathbf{F}_{(k,l)}(\mathbf{x}_{k-1}^l) + \mathbf{x}_{k-1}^l), \quad (5)$$

This can be explained by the fact that, after the addition of ReLU, it ensures a non-negative input to the subsequent residual unit. Consequently, the shortcut connection consistently maintains a non-negative status, and the convolutional layers are tasked with generating negative output prior to the addition process. This arrangement could potentially compromise the overall capability of the network architecture. Tackles this concern by introducing pre-activation residual units, where the Batch Normalization (BN) layer precedes ReLU (rather than following) the convolutional layer.

$$\mathbf{x}_k^l = (\mathbf{F}_{(k,l)}(\mathbf{x}_{k-1}^l) + \mathbf{x}_{k-1}^l), \quad (6)$$

In this approach, ReLU is eliminated after the addition process to establish an identity path. This modification leads to a considerable and substantial improvement in overall performance without encountering overfitting. Additionally, we identified that employing an extensive number of ReLU activations within each residual unit block can detrimentally affect performance, as illustrated in Figure 9.

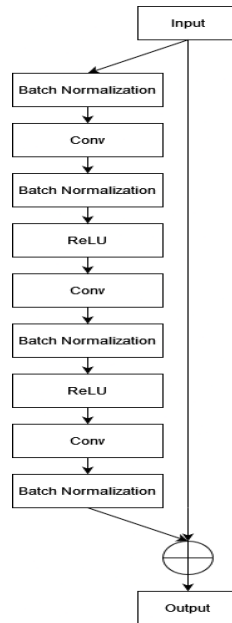


Figure 9: Illustration of using ReLU

3.8 Long Short-Term Memory (LSTM)

LSTM, an acronym for Long Short-Term Memory, allows for the processing of exceptionally lengthy input sequences. The emergence of LSTM as a solution stemmed from addressing the problem of gradient vanishing in traditional RNNs. LSTM is capable of retaining a set of information stored over a long period while simultaneously discarding irrelevant information. LSTM is more efficient in processing, predicting, and classifying data [Alazab et al., 20]. LSTM incorporates three gates: the input gate, the forget gate, and the output gate [Bintoro, 23]. The internal structure of LSTM is illustrated in Figure 10.

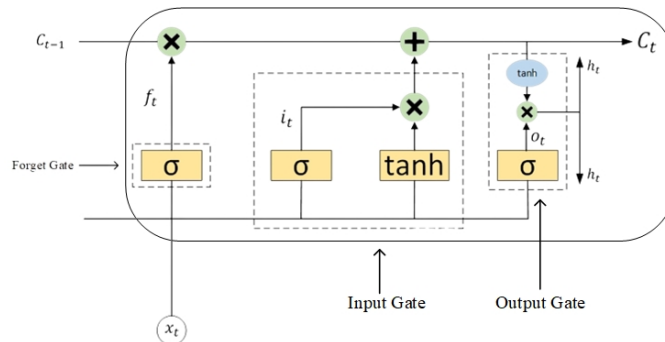


Figure 10: Structure of LSTM

The LSTM operations can be observed in the equations shown below:

$$f_t = \sigma_h(W_f x_t + U_f h_{t-1} + b_f) \quad (7)$$

$$i_t = \sigma_h(W_j x_t + U_j h_{t-1} + b_j) \quad (8)$$

$$o_t = \sigma_h(W_o x_t + U_o h_{t-1} + b_o) \quad (9)$$

$$c_t = f_t \odot c_{t-1} + i_t \odot \sigma_t(W_c x_t + U_c h_{t-1} + b_c) \quad (10)$$

$$h_t = o_t \odot \sigma_h(c_t) \quad (11)$$

Where f_t , i_t , o_t , c_t , h_t are activation vectors for each of the input gate, forget gate, output gate, cell state, and hidden state, respectively.

3.9 Evaluation Metrics

To assess the effectiveness of the proposed approach quantitatively, performance metrics including Accuracy, Precision, Recall, Sensitivity, Specificity, and F1-score are utilized. In our dataset, the categorization of Mpox as true positive (T_p) or true negative (T_n) occurs when individuals can correctly identify it. Conversely, it is classified as false positive (F_p) or false negative (F_n) [Alom et al., 20, Aslan, 22, Heidari et al., 20, Karthik et al., 21]. The specified statistical metrics are explained in detail below.

Accuracy represents the overall count of accurately identified cases among all cases. The calculation of accuracy can be derived using the following formula.

$$Accuracy = \frac{T_p + T_n}{T_p + T_n + F_p + F_n} \quad (12)$$

Precision is the proportion of correctly predicted positive outcomes relative to the total anticipated positive outcomes.

$$Precision = \frac{T_p}{T_p + F_p} \quad (13)$$

Recall pertains to the proportion of pertinent results correctly recognized by the algorithm.

$$Recall = \frac{T_p}{T_n + F_p} \quad (14)$$

Sensitivity is the metric that specifically measures accurate positives in comparison to the total occurrences.

$$Sensitivity = \frac{T_p}{T_p + F_n} \quad (15)$$

Specificity is the measure that identifies the accurately recognized actual negatives.

$$\text{Specificity} = \frac{T_n}{T_n + F_p} \quad (16)$$

The F1-score represents the harmonic mean between precision and recall. A perfect balance between precision and recall is indicated by the maximum achievable F1 score of 1.

$$F1 - score = 2 \times \frac{\text{Precision} \times \text{Recall}}{\text{Precision} + \text{Recall}} \quad (17)$$

4 Result

4.1 Model Training and Validation

In the experiment, the dataset was partitioned into 80% for training, 10% for validation, and 10% for testing. The implementation of the proposed model in this research was carried out using Jupyter notebook, Python, and libraries such as Keras and TensorFlow. The computational infrastructure supporting the study included an Intel® Core™ i7-2.8GHz processor, 16GB RAM, and a GPU GTX1060 with VRAM 6GB. The training dataset for the GAN comprised 228 images affected by Mpox and unaffected by Mpox, along with 2142 augmented images exhibiting either Mpox presence or absence. The GAN was trained for 1000 epochs, while the CNN-LSTM underwent training for 250 epochs, utilizing a 5 K-Fold Cross Validation approach. From the trained GAN model, 4752 synthetic Mpox images were generated, and 4500 images were selected from this set of 4752 images. The results of synthetic Mpox images using GAN are shown in Figure 11, and discriminant losses and adversary losses are depicted in Figure 12.

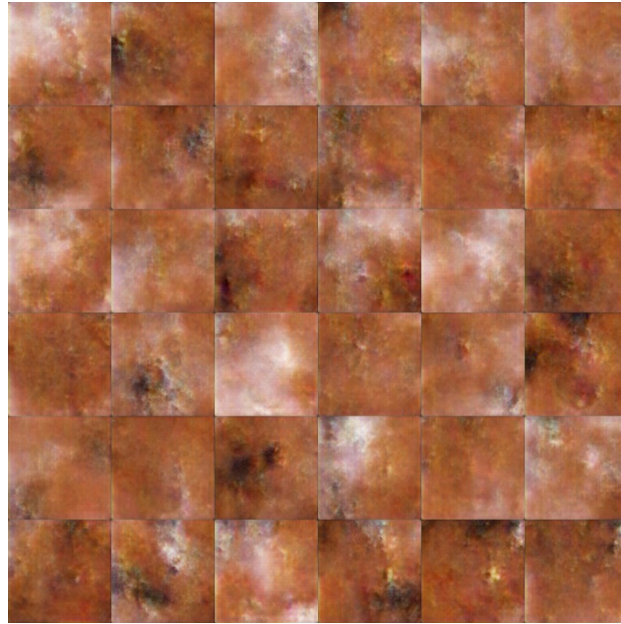


Figure 11: Mpx synthetic image generated by GAN

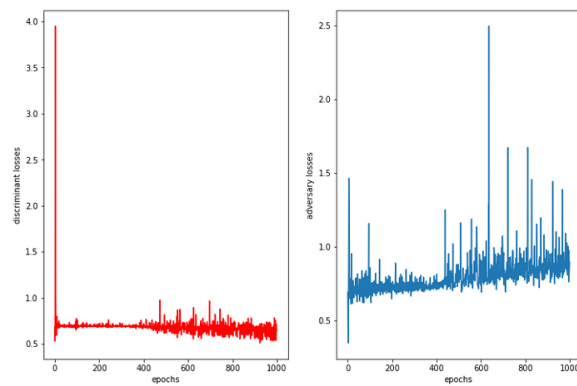


Figure 12: Training graphs produced by GAN (a) discriminant losses, (b) adversary losses

In addition to the artificially generated images, 30 Mpx images were incorporated into the Mpx CNN LSTM dataset. The remaining Mpx images were reserved for the evaluation and testing of the trained model. The architecture of the proposed GPLNet model underwent training using a dataset consisting of 81 images affected by Mpx, 100 images unaffected by Mpx, 784 augmented images affected by Mpx, and 930 augmented images unaffected by Mpx. The figures depicting the results of model comparison in terms of loss and accuracy are presented in Figures 13, 14, 15, and 16.

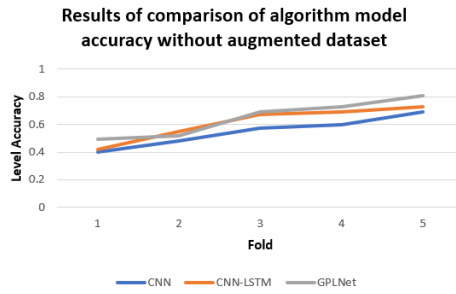


Figure 13: Result of comparison of algorithm model accuracy without augmented dataset

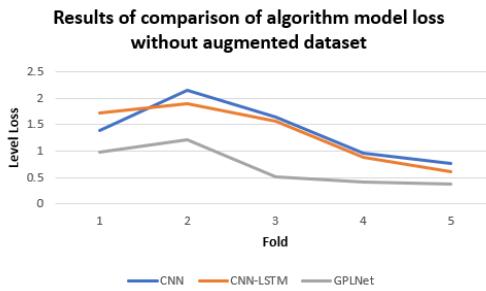


Figure 14: Result of comparison of algorithm model loss without augmented dataset

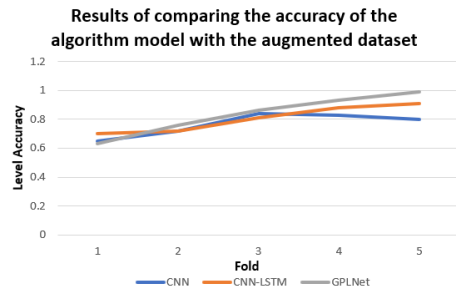


Figure 15: Result of comparison the accuracy of the algorithm model with the augmented dataset

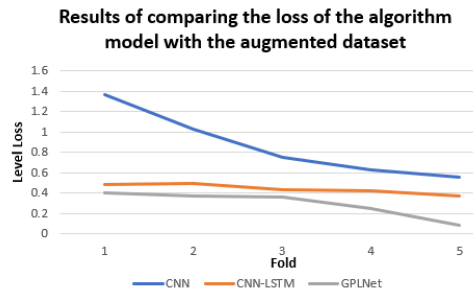


Figure 16: Result of comparison the loss of the algorithm model with the augmented dataset

To demonstrate the convergence of the model, the proposed GPLNet was evaluated using 5-fold cross-validation. Detailed results of the accuracy and loss comparison between the augmented dataset and the non-augmented dataset are shown in Table 3, Table 4, Table 5, and Table 6.

Fold	CNN	CNN-LSTM	GPLNet
1	0.4	0.42	0.49
2	0.48	0.55	0.52
3	0.57	0.67	0.69
4	0.6	0.69	0.73
5	0.69	0.73	0.81

Table 3: Results of accuracy comparison for the algorithm model without augmented dataset

Fold	CNN	CNN-LSTM	GPLNet
1	1.38	1.71	0.97
2	2.15	1.90	1.21
3	1.64	1.56	0.51
4	0.96	0.88	0.41
5	0.75	0.60	0.36

Table 4: Results of loss comparison for the algorithm model without augmented dataset

Fold	CNN	CNN-LSTM	GPLNet
1	0.65	0.7	0.63
2	0.72	0.72	0.76
3	0.84	0.81	0.86
4	0.83	0.88	0.93
5	0.8	0.91	0.99

Table 5: Results of accuracy comparison for the algorithm model with augmented dataset

Fold	CNN	CNN-LSTM	GPLNet
1	1.37	0.48	0.40
2	1.02	0.5	0.37
3	0.75	0.43	0.36
4	0.62	0.42	0.25
5	0.55	0.37	0.09

Table 6: Results of loss comparison for the algorithm model with augmented dataset

Figure 13 to Figure 16 depict the accuracy and loss curves for the CNN, CNN-LSTM, and GPLNet algorithm models with both augmented and non-augmented datasets. 5-Fold Cross Validation was employed to train accuracy and loss models for the simultaneously recorded training and validation datasets. To prevent overfitting in the model, we trained for up to 50 epochs for each fold, resulting in a total of 250 epochs used. The recorded training accuracy was 0.81 for the non-augmented dataset and 0.99 for the augmented dataset. The training loss was recorded as 0.36 for the non-augmented dataset and 0.09 for the augmented dataset.

4.2 Evaluation Metrics

The performance of the proposed algorithmic model is evaluated on the testing dataset. Accuracy, Precision, Recall, Sensitivity, Specificity, and F1-score are computed for each class as indicated in Table 7.

Data	1	2	3	4	5	6
Mpox	0.98	0.99	0.98	0.98	0.98	0.98
Others		0.99	0.98	0.98	0.98	0.98

Note:

1=Accuracy, 2=Precision, 3=Recall, 4=Sensitivity, 5=Specificity, 6=F1-score

Table 7: Performance metrics (Accuracy, Precision, Recall, Sensitivity, Specificity, and F1-score) for each test class

The outcomes of the study showcase notable accuracy across all classes in the independent test dataset, with an accuracy score of 0.98, precision reaching 0.99, recall at 0.98, Sensitivity measuring 0.98, Specificity at 0.98, and an f1-score of 0.98. The Receiver Operating Characteristic (ROC) serves as a graphical representation depicting the performance of the classification model across diverse threshold values. The ROC curve illustrates the true positive rate plotted against the false positive rate at each threshold setting [Movahedi et al., 23]. The ROC and AUC for Mpox is 0.99, and for others, it is 0.99, as shown in Figure 17, while Figure 18 illustrates the confusion matrix.

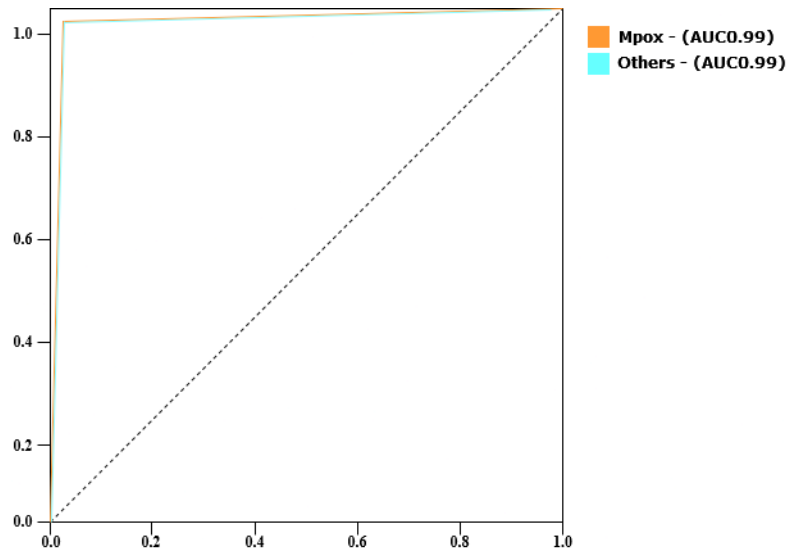


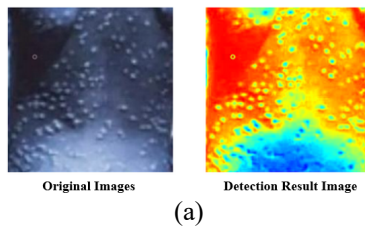
Figure 17: ROC and AUC curve results of the proposed algorithm model

Predicted Label	Mpx	212	1
	Others	2	115
		Mpx	Others
		Actual Label	

Figure 18: Confusion matrix results from the proposed algorithm model

4.3 Result of Disease Detection

After the algorithmic model successfully classified and identified Mpx disease, the algorithmic model also detected diseases, as illustrated in Figure 19.



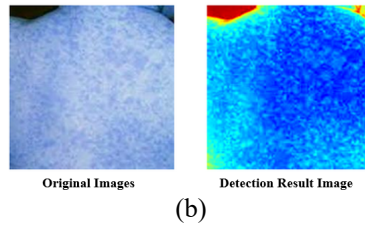


Figure 19: Result of disease detection (a) Mpx, (b) others

Visualization of Mpx disease detection results using the GPLNet model. This stage aims to analyze the performance of the trained and tested model. In Figure 19, it is illustrated that the highlighted areas in orange and yellow indicate the regions of Mpx disease.

4.4 Comparison of CNN, CNN-LSTM, and GPLNet Model Algorithms Against Actual Disease Status

Figure 20 shows the comparison curve of the confidence level of the CNN, CNN-LSTM, and GPLNet algorithmic models against the actual disease status. Table 8 provides details of the confidence level of the CNN, CNN-LSTM, and GPLNet algorithmic models against the actual disease status.

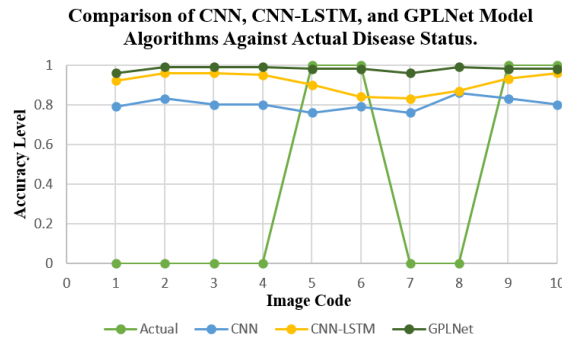


Figure 20: Comparison curve of confidence level of CNN, CNN-LSTM, and GPLNet algorithm models on actual disease status.

1	2	3	4	5	6	7	8	9	10	11
I-1	0	0.79	0.92	0.96	1	Others	0	Mpx	0	Mpx
I-2	0	0.83	0.96	0.99	0	Mpx	0	Mpx	0	Mpx
I-3	0	0.8	0.96	0.99	0	Mpx	0	Mpx	0	Mpx
I-4	0	0.8	0.95	0.99	1	Others	0	Mpx	0	Mpx
I-5	1	0.76	0.9	0.98	0	Mpx	1	Others	1	Others
I-6	1	0.79	0.84	0.98	0	Mpx	0	Mpx	1	Others
I-7	0	0.76	0.83	0.96	1	Others	0	Mpx	0	Mpx

I-8	0	0.86	0.87	0.99	1	Others	1	Others	0	Mpox
I-9	1	0.83	0.93	0.98	0	Mpox	0	Mpox	1	Others
I-10	1	0.8	0.96	0.98	1	Others	1	Others	1	Others

Note: 1= Image Code, 2= Actual, 3= CNN Confidence, 4= CNN-LSTM Confidence, 5= GPLNet Confidence, 6= CNN Detection, 7= CNN Validation Against Actual, 8= CNN-LSTM Detection, 9= CNN-LSTM Validation Against Actual, 10= GPLNet Detection, 11= GPLNET Validation Against Actual

Table 8: Details of the level of confidence of the CNN, CNN-LSTM, and GPLNet algorithm models regarding the actual disease status.

4.5 Comparison of Result Achieved with Previous Works

We conducted a comparison of results from several literature references that serve as references in this study. We compared several metrics such as accuracy, precision, recall, sensitivity, specificity, and F1-score. Table 9 shows the comparison of results achieved with previous works.

Previous Works	Accuracy	Precision	Recall	Sensitivity	Specificity	F1-score
[Dahiya et al., 23]	98.18%	99.1%	92.8%	-	-	-
[Sitaula & Shahi, 22]	87.13%	85.44%	85.47%	-	-	85.40%
[Sorayaie Azar et al., 23]	97.63%	89.96%	98.89%	91.08%	98.47%	90.51%
[Jaradat et al., 2023]	98.16%	99%	96%	-	-	98%
[Eliwa et al., 23]	95.31%	95.63%	98.14%	-	-	96.87%
This Research	98%	99%	98%	98%	98%	98%

Table 9: Comparison of result achieved with previous works.

The proposed system has shown promising results compared to previous works. Table 9 displays the testing outcomes with the highest accuracy of 98%. Based on the comparison conducted with various evaluation metrics, it is concluded that the proposed model, GPLNet, surpasses previous research.

5 Conclusions and future work

This research introduces a novel algorithmic model designed 23ft he23 automated detection of systemic diseases, specifically targeting the identification 23ft he Mpox virus through the analysis of skin lesions. Achieving an impressive success rate of 98%

after comprehensive training, the developed technique emerges as a rapid and efficient automated detection tool. Moreover, it demonstrates the capability to distinguish between Mpox and non-Mpox systemic diseases. The distinguishing features in skin lesion images between these two categories often lie in the intricate details. Consequently, a substantial collection of high-resolution images becomes crucial for accurate recognition. Leveraging the rapidly evolving GAN model, high-resolution synthetic images are generated to address this requirement. Subsequently, a sophisticated PyramidalNet CNN model, deeply layered, is proposed, and integrated with LSTM. This model is trained using a combination of synthetic images from GAN and authentic images obtained from publicly available datasets, resulting in remarkable accuracy. The research findings underscore that the GPLNet algorithmic model surpasses the accuracy achieved by conventional CNN and CNN-LSTM, registering an impressive 0.99/99%. The performance of the GPLNet algorithmic model is further evaluated using multiple metrics, yielding accuracy, precision, recall, sensitivity, specificity, F1-score, and ROC values of 0.98, 0.99, 0.98, 0.98, 0.98, 0.98, 0.98, 0.98, and 0.99, respectively.

Future research may lead to the development of an Android-based application. The developed application aims to facilitate healthcare professionals in detecting Mpox disease, thereby enabling early intervention for the disease.

6 Future Work

The upcoming research requires the implementation of an application to assist doctors in detecting Mpox disease.

Acknowledgements

Not applicable.

References

- [Aggarwal et al., 21] Aggarwal, A., Mittal, M., & Battineni, G. (2021). Generative adversarial network: An overview of theory and applications. *International Journal of Information Management Data Insights*, 1(1). <https://doi.org/10.1016/j.jjime.2020.100004>
- [Ahsan et al., 20] Ahsan, M., Gupta, K. D., Islam, M. M., & Sen, S. (2020). COVID-19 Symptoms Detection Based on NasNetMobile with Explainable AI Using Various Imaging Modalities. 490–504. <https://doi.org/10.3390/make2040027>
- [Ahsan et al., 23] Ahsan, M. M., Ali, M. S., Hassan, M. M., Abdullah, T. A., Gupta, K. D., Bagci, U., Kaushal, C., & Soliman, N. F. (2023). Monkeypox Diagnosis with Interpretable Deep Learning. *IEEE Access*, 11(August), 81965–81980. <https://doi.org/10.1109/ACCESS.2023.3300793>
- [Ahsan, et al., 23] Ahsan, M. M., Uddin, M. R., Ali, M. S., Islam, M. K., Farjana, M., Sakib, A. N., Momin, K. Al, & Luna, S. A. (2023). Deep transfer learning approaches for Monkeypox disease diagnosis. *Expert Systems with Applications*, 216(January), 119483. <https://doi.org/10.1016/j.eswa.2022.119483>

- [Akkilic et al., 24] Akkilic, A. N., Sabir, Z., Bhat, S. A., & Bulut, H. (2024). A radial basis deep neural network process using the Bayesian regularization optimization for the monkeypox transmission model. *Expert Systems with Applications*, 235(August 2023), 121257. <https://doi.org/10.1016/j.eswa.2023.121257>
- [Alazab et al., 20] Alazab, M., Awajan, A., Mesleh, A., Abraham, A., Jatana, V., & Alhyari, S. (2020). COVID-19 prediction and detection using deep learning. *International Journal of Computer Information Systems and Industrial Management Applications*, 12(April), 168–181.
- [Allan-Blitz & Klausner, 23] Allan-Blitz, L. T., & Klausner, J. D. (2023). Current Evidence Demonstrates That Monkeypox Is a Sexually Transmitted Infection. *Sexually Transmitted Diseases*, 50(2), 63–65. <https://doi.org/10.1097/OLQ.0000000000001705>
- [Alom et al., 20] Alom, M. Z., Rahman, M. M. S., Nasrin, M. S., Taha, T. M., & Asari, V. K. (2020). COVID_MTNNet: COVID-19 Detection with Multi-Task Deep Learning Approaches. <http://arxiv.org/abs/2004.03747>
- [Altun et al., 23] Altun, M., Gürüler, H., Özkaraca, O., Khan, F., Khan, J., & Lee, Y. (2023). Monkeypox Detection Using CNN with Transfer Learning. *Sensors*, 23(4). <https://doi.org/10.3390/s23041783>
- [Arden and Chilcot, 20] Arden, M. A., & Chilcot, J. (2020). Health psychology and the coronavirus (COVID-19) global pandemic: A call for research. *British Journal of Health Psychology*, 25(2), 231–232. <https://doi.org/10.1111/bjhp.12414>
- [Ardila et al., 23] Ardila, Carlos M, Arrubla-Escobar, Daniel Esteban, Vivares-Builes, A. M. (2023). Oral lesions in patients with human monkeypox: A systematic scoping review. *Journal of Oral Pathology & Medicine*, 52(6), 459–467. <https://doi.org/10.1111/jop.13375>
- [Aslan, 22] Aslan, M. F. (2022). A robust semantic lung segmentation study for CNN-based COVID-19 diagnosis. *Chemometrics and Intelligent Laboratory Systems*, 231(October), 104695. <https://doi.org/10.1016/j.chemolab.2022.104695>
- [Bala et al., 23] Bala, D., Hossain, M. S., Hossain, M. A., Abdullah, M. I., Rahman, M. M., Manavalan, B., Gu, N., Islam, M. S., & Huang, Z. (2023). MonkeyNet: A robust deep convolutional neural network for monkeypox disease detection and classification. *Neural Networks*, 161, 757–775. <https://doi.org/10.1016/j.neunet.2023.02.022>
- [Baudouin et al., 23] Baudouin, R., Vallée, A., Zucman, D., & Hans, S. (2023). Detection of Monkeypox Virus in 2 Cases of Oral Sexually Transmitted Infection. *Ear, Nose and Throat Journal*. <https://doi.org/10.1177/01455613231175786>
- [Bibi et al., 23] Bibi, S., Khan, M. A., Shah, J. H., Damaševičius, R., Alasiry, A., Marzougui, M., Alhaisoni, M., & Masood, A. (2023). MSRNet: Multiclass Skin Lesion Recognition Using Additional Residual Block Based Fine-Tuned Deep Models Information Fusion and Best Feature Selection. *Diagnostics*, 13(19), 1–22. <https://doi.org/10.3390/diagnostics13193063>
- [Bintoro, 23] Bintoro, P. (2023). APPLICATION OF LUNG DISEASES DETECTION BASED ON CSLNet *Jurnal Nasional Pendidikan Teknik Informatika : JANAPATI* | 438. 12(3), 437–450.
- [Chadaga et al., 23] Chadaga, K., Prabhu, S., Sampathila, N., Nireswalya, S., Katta, S. S., Tan, R. S., & Acharya, U. R. (2023). Application of Artificial Intelligence Techniques for Monkeypox: A Systematic Review. *Diagnostics*, 13(5), 1–16. <https://doi.org/10.3390/diagnostics13050824>

- [Chai et al., 21] Chai, J., Zeng, H., Li, A., & Ngai, E. W. T. (2021). Machine Learning with Applications Deep learning in computer vision: A critical review of emerging techniques and application scenarios. *Machine Learning with Applications*, 6(August), 100134. <https://doi.org/10.1016/j.mlwa.2021.100134>
- [Chastain et al., 2023] Chastain, Daniel B.; Motoa, Gabriel; Ortiz-Martínez, Yeimer; Gharamti, Amal; Henao-Martínez, A. F. . (2023). Characteristics and clinical manifestations of monkeypox among people with and without HIV in the United States: a retrospective cohort. *Wolters Kluwer*, 37(4), 611–616. <https://doi.org/10.1097/QAD.0000000000003449>
- [Chen et al., 20] Chen, J., Wang, R., Wang, M., & Wei, G. W. (2020). Mutations Strengthened SARS-CoV-2 Infectivity. *Journal of Molecular Biology*, 432(19), 5212–5226. <https://doi.org/10.1016/j.jmb.2020.07.009>
- [Chhabra et al., 23] Chhabra, M., Kumar, K., Manoj, R., Abhay, K., & Anand, S. (2023). Improving automated latent fingerprint detection and segmentation using deep convolutional neural network. *Neural Computing and Applications*, 35(9), 6471–6497. <https://doi.org/10.1007/s00521-022-07894-y>
- [Dahiya et al., 23] Dahiya, N., Sharma, Y. K., Rani, U., Hussain, S., Nabilal, K. V., Mohan, A., & Nuristani, N. (2023). Hyper-parameter tuned deep learning approach for effective human monkeypox disease detection. *Scientific Reports*, 13(1), 1–18. <https://doi.org/10.1038/s41598-023-43236-1>
- [Dhungel et al., 20] Dhungel, P., Cantu, F. M., Molina, J. A., & Yang, Z. (2020). Vaccinia virus as a master of host shutoff induction: Targeting processes of the central dogma and beyond. *Pathogens*, 9(5). <https://doi.org/10.3390/pathogens9050400>
- [Dimitrakoff et al., 22] Dimitrakoff, J., Thornhill, J. P., & Antinori, A. (2022). Monkeypox Virus Infection across 16 Countries — April–June 2022. *New England Journal of Medicine*, 387(25), e69. <https://doi.org/10.1056/nejmc2213969>
- [Eeuwijk, 22] Eeuwijk, F. Van. (2022). *Multivariate Statistical Machine Learning Methods for Genomic Prediction*.
- [Eliwa et al., 23] Eliwa, E. H. I., El Koshiry, A. M., Abd El-Hafeez, T., & Farghaly, H. M. (2023). Utilizing convolutional neural networks to classify monkeypox skin lesions. *Scientific Reports*, 13(1), 1–20. <https://doi.org/10.1038/s41598-023-41545-z>
- [Ethawi et al., 23] Ethawi, Y., Kheder, R. M., Huseynova, R., Singh, S., Dana, A., Baiti, N. Al, Alzir, R., Mozibur, R. M., Kasniya, G., & Ali, Y. (2023). *Journal of Pediatrics & Neonatal Biology*. 8(3), 226–232.
- [Gigante et al., 22] Gigante, C. M., Korber, B., Seabolt, M. H., Wilkins, K., Davidson, W., Rao, A. K., Zhao, H., Smith, T. G., Hughes, C. M., Minhaj, F., Waltenburg, M. A., Theiler, J., Smole, S., Gallagher, G. R., Blythe, D., Myers, R., Schulte, J., Stringer, J., Lee, P., ... Li, Y. (2022). Multiple lineages of monkeypox virus detected in the United States, 2021–2022. *Science*, 378(6619), 560–565. <https://doi.org/10.1126/science.add4153>
- [Gui et al., 23] Gui, J., Member, S., Sun, Z., & Member, S. (2023). A Review on Generative Adversarial Networks: Algorithms , Theory , and Applications. *IEEE Transactions on Knowledge and Data Engineering*, 35(4), 3313–3332. <https://doi.org/10.1109/TKDE.2021.3130191>
- [Gulakala et al., 23] Gulakala, R., Markert, B., & Stoffel, M. (2023). Rapid diagnosis of Covid-19 infections by a progressively growing GAN and CNN optimisation. *Computer Methods and Programs in Biomedicine*, 229, 107262. <https://doi.org/10.1016/j.cmpb.2022.107262>

- [Heidari et al., 20] Heidari, M., Mirniaharikandehei, S., Khuzani, A. Z., Danala, G., Qiu, Y., & Zheng, B. (2020). Improving the performance of CNN to predict the likelihood of COVID-19 using chest X-ray images with preprocessing algorithms. *International Journal of Medical Informatics*, 144(September), 104284. <https://doi.org/10.1016/j.ijmedinf.2020.104284>
- [Hemati et al., 22] Hemati, S., Farhadkhani, M., Sanami, S., & Mohammadi-Moghadam, F. (2022). A review on insights and lessons from COVID-19 to the prevent of monkeypox pandemic. *Travel Medicine and Infectious Disease*, 50(June), 102441. <https://doi.org/10.1016/j.tmaid.2022.102441>
- [Hussain et al., 23] Hussain, M., Khan, M. A., Damaševičius, R., Alasiry, A., Marzougui, M., Alhaisoni, M., & Masood, A. (2023). SkinNet-INIO: Multiclass Skin Lesion Localization and Classification Using Fusion-Assisted Deep Neural Networks and Improved Nature-Inspired Optimization Algorithm. *Diagnostics*, 13(18). <https://doi.org/10.3390/diagnostics13182869>
- [Hussein et al., 22] Hussein, F., Mughaid, A., AlZu'bi, S., El-Salhi, S. M., Abuhaija, B., Abualigah, L., & Gandomi, A. H. (2022). Hybrid CLAHE-CNN Deep Neural Networks for Classifying Lung Diseases from X-ray Acquisitions. *Electronics*, 11(19), 3075. <https://doi.org/10.3390/electronics11193075>
- [Ijaz et al., 23] Ijaz, M. A., Abid, M. K., Aslam, N., & Mudaseer, A. Q. (2023). Detecting Monkeypox in humans using deep learning. 11(2), 265–272.
- [Jain et al., 20] Jain, R., Nagrath, P., Kataria, G., Kaushik, V. S., & Hemanth, D. J. (2020). Pneumonia detection in chest X-ray images using convolutional neural networks and transfer learning. *Measurement*, 165, 108046. <https://doi.org/10.1016/j.measurement.2020.108046>
- [Jaradat et al., 23] Jaradat, A. S., Al Mamlook, R. E., Almakayeel, N., Alharbe, N., Almuflih, A. S., Nasayreh, A., Gharaibeh, H., Gharaibeh, M., Gharaibeh, A., & Bzizi, H. (2023). Automated Monkeypox Skin Lesion Detection Using Deep Learning and Transfer Learning Techniques. *International Journal of Environmental Research and Public Health*, 20(5). <https://doi.org/10.3390/ijerph20054422>
- [Jiao et al., 20] Jiao, Y., Deng, Y., Luo, Y., & Lu, B. (2020). Driver sleepiness detection from EEG and EOG signals using GAN and LSTM networks. 408, 100–111. <https://doi.org/10.1016/j.neucom.2019.05.108>
- [Jiao & Jiang, 22] Jiao, Y., & Jiang, F. (2022). Detecting slow eye movements with bimodal-LSTM for recognizing drivers' sleep onset period. *Biomedical Signal Processing and Control*, 75(March), 103608. <https://doi.org/10.1016/j.bspc.2022.103608>
- [Joseph & Anil, 23] Joseph, B., & Anil, S. (2023). Oral lesions in human monkeypox disease and their management—a scoping review. *Oral Surgery, Oral Medicine, Oral Pathology and Oral Radiology*, 135(4), 510–517. <https://doi.org/10.1016/j.oooo.2022.11.012>
- [Karagoz et al., 23] Karagoz, A., Tombuloglu, H., Alsaeed, M., Tombuloglu, G., AlRubaish, A. A., Mahmoud, A., Smajlović, S., Ćordić, S., Rabaan, A. A., & Alsuhaimi, E. (2023). Monkeypox (mpox) virus: Classification, origin, transmission, genome organization, antiviral drugs, and molecular diagnosis. *Journal of Infection and Public Health*, 16(4), 531–541. <https://doi.org/10.1016/j.jiph.2023.02.003>
- [Karthik et al., 21] Karthik, R., Menaka, R., & Hariharan, M. (2021). Learning distinctive filters for COVID-19 detection from chest X-ray using shuffled residual CNN. *Applied Soft Computing*, 99, 106744. <https://doi.org/10.1016/j.asoc.2020.106744>
- [Li et al., 21] Li, Y., Wang, Q., Zhang, J., Hu, L., & Ouyang, W. (2021). Neurocomputing The theoretical research of generative adversarial networks : an overview. *Neurocomputing*, 435, 26–41. <https://doi.org/10.1016/j.neucom.2020.12.114>

- [Mahdy et al., 22] Mahdy, L. N., El Seddawy, A. I. B., & Ezzat, K. A. (2022). Automatic COVID-19 lung images classification system based on convolution neural network. *International Journal of Electrical and Computer Engineering*, 12(5), 5573–5579. <https://doi.org/10.11591/ijece.v12i5.pp5573-5579>
- [Maqsood & Damaševičius, 23] Maqsood, S., & Damaševičius, R. (2023). Monkeypox Detection and Classification Using Deep Learning Based Features Selection and Fusion Approach. *SysCon 2023 - 17th Annual IEEE International Systems Conference, Proceedings*, 1–8. <https://doi.org/10.1109/SysCon53073.2023.10131067>
- [Meena et al., 23] Meena, G., Mohbey, K. K., Kumar, S., & Lokesh, K. (2023). A hybrid deep learning approach for detecting sentiment polarities and knowledge graph representation on monkeypox tweets. *Decision Analytics Journal*, 7(May), 100243. <https://doi.org/10.1016/j.dajour.2023.100243>
- [Mitjà et al., 23] Mitjà, O., Ogoina, D., Titanji, B. K., Galvan, C., Muyembe, J.-J., Marks, M., & Orkin, C. M. (2023). Monkeypox. *Lancet* (London, England), 401(10370), 60–74. [https://doi.org/10.1016/S0140-6736\(22\)02075-X](https://doi.org/10.1016/S0140-6736(22)02075-X)
- [Movahedi et al., 23] Movahedi, F., Padman, R., & Antaki, J. F. (2023). Limitations of receiver operating characteristic curve on imbalanced data: Assist device mortality risk scores. *Journal of Thoracic and Cardiovascular Surgery*, 165(4), 1433-1442.e2. <https://doi.org/10.1016/j.jtcvs.2021.07.041>
- [My et al., 21] My, D., Manh, D., Phuong, T., & Lee, S. (2021). HI-GAN: A hierarchical generative adversarial network for blind denoising of real photographs. *Information Sciences*, 570, 225–240. <https://doi.org/10.1016/j.ins.2021.04.045>
- [Nayak et al., 23] Nayak, T., Chadaga, K., Sampathila, N., Mayrose, H., Gokulkrishnan, N., Bairy G, M., Prabhu, S., S, S. K., & Umakanth, S. (2023). Deep learning based detection of monkeypox virus using skin lesion images. *Medicine in Novel Technology and Devices*, 18(May), 100243. <https://doi.org/10.1016/j.medntd.2023.100243>
- [Nguyen et al., 21] Nguyen, P. Y., Ajisegiri, W. S., Costantino, V., Chughtai, A. A., & MacIntyre, C. R. (2021). Reemergence of human monkeypox and declining population immunity in the context of urbanization, Nigeria, 2017-2020. *Emerging Infectious Diseases*, 27(4), 1007–1014. <https://doi.org/10.3201/eid2704.203569>
- [Nivedha & Shankar, 23] Nivedha, S., & Shankar, S. (2023). Melanoma Diagnosis Using Enhanced Faster Region Convolutional Neural Networks Optimized by Artificial Gorilla Troops Algorithm. *Information Technology and Control*, 52(4), 819–832. <https://doi.org/10.5755/j01.itc.52.4.33503>
- [Othmani et al., 23] Othmani, A., Qalid, A., Aslan, S., Chaieb, F., Rameh, H., Alfred, R., & Cohen, D. (2023). EEG-based neural networks approaches for fatigue and drowsiness detection : A survey. *Neurocomputing*, 557(August), 126709. <https://doi.org/10.1016/j.neucom.2023.126709>
- [Paharia, 22] Paharia, P. T. (2022). Insights into the biology of the monkeypox virus. In *News-Medical*. <https://www.news-medical.net/news/20220823/Insights-into-the-biology-of-the-monkeypox-virus.aspx>
- [Paul et al., 22] Paul, J., Ahmed, M. T., & Tasnim Jahan Peana. (2022). Monkeypox Skin Lesion Dataset. <https://www.kaggle.com/datasets/nafin59/monkeypox-skin-lesion-dataset>

[Pfäfflin et al., 23] Pfäfflin, F., Wendisch, D., Scherer, R., Jürgens, L., Godzick, G., Eva, N., Tober, P., Miriam, L., Stegemann, S., Max, V., Florian, C., Dirk, K., & Kurth, F. (2023). Monkeypox in - patients with severe anal pain. *Infection*, 51(2), 483–487. <https://doi.org/10.1007/s15010-022-01896-7>

[Pittman et al., 22] Pittman, P. R., Martin, J. W., Kingebeni, P. M., Tamfum, J. M., Wan, Q., Reynolds, M. G., Quinn, X., Norris, S., Townsend, M. B., Panayampalli, S., Reed, W., & Military, N. (2022). Clinical characterization of human monkeypox infections in the Democratic Republic of the Congo Short Title: Clinical characterization of human monkeypox infection.

[Sitaula & Shahi, 22] Sitaula, C., & Shahi, T. B. (2022). Monkeypox Virus Detection Using Pre-trained Deep Learning-based Approaches. *Journal of Medical Systems*, 46(11). <https://doi.org/10.1007/s10916-022-01868-2>

[Sorayaie Azar et al., 23] Sorayaie Azar, A., Naemi, A., Babaei Rikan, S., Bagherzadeh Mohasefi, J., Pirnejad, H., & Wiil, U. K. (2023). Monkeypox detection using deep neural networks. *BMC Infectious Diseases*, 23(1), 1–13. <https://doi.org/10.1186/s12879-023-08408-4>

[Stojanov, 21] Stojanov, D. (2021). Phylogenicity of B.1.1.7 surface glycoprotein, novel distance function and first report of V90T missense mutation in SARS-CoV-2 surface glycoprotein. *Meta Gene*, 30(August), 100967. <https://doi.org/10.1016/j.mgene.2021.100967>

[Stojanov, 23] Stojanov, D. (2023). Structural implications of SARS-CoV-2 Surface Glycoprotein N501Y mutation within receptor-binding domain [499-505]—computational analysis of the most frequent Asn501 polar uncharged amino acid mutations. *Biotechnology and Biotechnological Equipment*, 37(1). <https://doi.org/10.1080/13102818.2023.2206492>

[Studemeister et al., 23] Studemeister, L., Pai, S., Walsh, K., & Cooper, J. (2023). Communications: Adult. *Journal of Emergency Medicine*, 64(2), 211–213. <https://doi.org/10.1016/j.jemermed.2022.12.029>

[Valero, 23] Valero, P. (2023). Urology Case Reports Penile necrosis due to monkeypox. 51(August), 4–7. <https://doi.org/10.1016/j.eucr.2023.102554>

[Velu et al., 23] Velu, M., Dhanaraj, R. K., Balusamy, B., Kadry, S., Yu, Y., Nadeem, A., & Rauf, H. T. (2023). Human Pathogenic Monkeypox Disease Recognition Using Q-Learning Approach. *Diagnostics*, 13(8). <https://doi.org/10.3390/diagnostics13081491>

[Waheed et al., 20] Waheed, A., Goyal, M., Gupta, D., Khanna, A., Al-Turjman, F., & Pinheiro, P. R. (2020). CovidGAN: Data Augmentation Using Auxiliary Classifier GAN for Improved Covid-19 Detection. *IEEE Access*, 8, 91916–91923. <https://doi.org/10.1109/ACCESS.2020.2994762>

[Xiang and White, 22] Xiang, Y., & White, A. (2022). Monkeypox virus emerges from the shadow of its more infamous cousin: family biology matters. *Emerging Microbes and Infections*, 11(1), 1768–1777. <https://doi.org/10.1080/22221751.2022.2095309>

[Yang et al., 21] Yang, D. Q., Li, T., Liu, M. T., Li, X. W., & Chen, B. H. (2021). A systematic study of the class imbalance problem: Automatically identifying empty camera trap images using convolutional neural networks. *Ecological Informatics*, 64(April), 101350. <https://doi.org/10.1016/j.ecoinf.2021.101350>

[W. T. Yang et al., 22] Yang, W. T., Huang, W. H., Liao, T. L., Hsiao, T. H., Chuang, H. N., & Liu, P. Y. (2022). SARS-CoV-2 E484K Mutation Narrative Review: Epidemiology, Immune Escape, Clinical Implications, and Future Considerations. *Infection and Drug Resistance*, 15(February), 373–385. <https://doi.org/10.2147/IDR.S344099>

[Zhugunissov et al., 23] Zhugunissov, K., Mambetaliyev, M., Sarsenkulova, N., Tabys, S., Kenzhebaeva, M., Issimov, A., & Abduraimov, Y. (2023). Development of an Inactivated Camel-pox Vaccine from Attenuated Camel-pox Virus Strain: Safety and Protection in Camels. *Animals*, 13(9). <https://doi.org/10.3390/ani13091513>